In *Small-Scale Structures in Three-Dimensional Hydrodynamic and Magnetohydrodynamic Turbulence*, Proceedings of a workshop held at Nice, France, 10–13 Jan, 1995. M. Meneguzzi, A. Pouquet, and P.-L. Sulem (eds). Lecture Notes in Physics, Vol. 462. Springer, 1995. ISBN 3-540-60486-3.

Anisotropy in Incompressible and Compressible 3D MHD Turbulence

Sean Oughton[1], *William H. Matthaeus*[2] *and Sanjoy Ghosh*[3]

[1] Department of Mathematics, University College London, Gower Street, London WC1E 6BT, England
[2] Bartol Research Institute, University of Delaware, Newark, DE 19716, USA
[3] USRA, Goddard Space Flight Center, Greenbelt, MD 20771, USA

Abstract

Using direct numerical simulation results we discuss how the presence of a dc magnetic field ($\mathbf{B}_0$) in initially isotropic turbulent magnetohydrodynamic (MHD) flows leads to anisotropy in the small-scale velocity and magnetic fields. In such cases, the small-scale vorticity and current structures tend to elongate and align with $\mathbf{B}_0$.

The incompressible behaviour is also compared to weakly compressible results (sonic Mach number < 0.5). The simulations indicate that while density and longitudinal pressure fluctuations remain isotropic for the compressible systems, the $\mathbf{v}$ and $\mathbf{b}$ fluctuations behave quite similarly to their incompressible counterparts, exhibiting substantial anisotropies even at the modest Reynolds numbers employed here.

1 Introduction

Numerical studies of freely decaying 2D MHD turbulence in the presence of a uniform and constant magnetic field, $\mathbf{B}_0$ (in the plane of the turbulence), indicated that turbulent states which were initially isotropic quickly became anisotropic [1]. Excitations were preferentially transferred to the modes with wavevectors ($\mathbf{k}$) perpendicular to $\mathbf{B}_0$, relative to the parallel modes. It was conjectured in [1] that similar trends and features would be seen in the evolution of 3D incompressible flows. Here we use direct numerical simulation (DNS) to verify this conjecture, and present initial results suggesting that similar behaviour also occurs in weakly compressible 3D MHD flows.

Our results were obtained via spectral simulation of the incompressible 3D MHD equations for the solenoidal zero-mean velocity ($\mathbf{v}$) and magnetic ($\mathbf{b}$) fields, with $\mathbf{B}_0 = B_0\,\hat{\mathbf{z}}$,

$$\frac{\partial \mathbf{v}}{\partial t} + \mathbf{v}\cdot\nabla\mathbf{v} = -\nabla p^* + \mathbf{b}\cdot\nabla\mathbf{b} + \mathbf{B}_0\cdot\nabla\mathbf{b} + \nu\nabla^2\mathbf{v}, \tag{1}$$

$$\frac{\partial \mathbf{b}}{\partial t} + \mathbf{v}\cdot\nabla\mathbf{b} = \mathbf{b}\cdot\nabla\mathbf{v} + \mathbf{B}_0\cdot\nabla\mathbf{v} + \eta\nabla^2\mathbf{b}. \tag{2}$$

The variables have their usual meanings, with current density $\mathbf{j} = \nabla \times \mathbf{b}$, vorticity $\boldsymbol{\omega} = \nabla \times \mathbf{v}$, kinetic and magnetic energies per unit mass $E^v = \langle \mathbf{v}^2/2 \rangle$, $E^b = \langle \mathbf{b}^2/2 \rangle$, total energy $E = E^v + E^b$, and cross and magnetic helicities $H_c = \langle \mathbf{v} \cdot \mathbf{b} \rangle/2$, $H_m = \langle \mathbf{a} \cdot \mathbf{b} \rangle/2$, where $\mathbf{b} = \nabla \times \mathbf{a}$. Angle brackets denote averaging over the spatial domain. Time is measured in large-scale eddy turnover times.

The (discrete) Fourier decompositions of these fields are also of use, e.g., $\mathbf{v}(\mathbf{x}, t) = \sum_{\mathbf{k}} \mathbf{v}(\mathbf{k}, t) \exp(\mathrm{i}\, \mathbf{k} \cdot \mathbf{x})$, where the wavevectors $\mathbf{k}$ have integer components since we solve in a periodic cube of side 2π. Spectra are denoted by $E^v(k)$, etc. The runs discussed here retain 64 Fourier modes in each Cartesian direction. Further details regarding the computational setup and the incompressible results are given in [2].

2 Incompressible Results

We consider results from five runs. In each case the initial conditions were identical, only the value of B_0 being varied from run to run. The $\mathbf{v}$ and $\mathbf{b}$ fields were generated using Gaussian random variables subject to the constraints $H_m, H_c \approx 0$, $E = 1$, and equipartition of the kinetic and magnetic energy at each excited wavenumber. Modes with wavenumbers from $k = 1$–8 were excited. The inverse (large-scale) Reynolds numbers are $\nu = \eta = 1/200$. The specific values of B_0 used were: 0, 0.1, 1, 3, and 8. We consider first the evolution of bulk quantities and then introduce a set of anisotropy diagnostics.

Time histories of the globals show qualitatively similar behaviour across runs; nonetheless, several trends are observed. Figure 1(a) shows E^v, E^b, and E for the $B_0 = 0$ run. It is seen that an excess of E^b quickly arises. As B_0 is increased, however, this excess is progressively reduced until approximate equipartition is once again achieved. This can be understood in terms of the Alfvén effect [3, 4], wherein the small-scale fluctuations are assumed to behave like Alfvén waves which, on average, have equal amounts of kinetic and magnetic energy. A second trend involves the decrease of the maxima of the enstrophy, $\Omega = \langle \boldsymbol{\omega}^2 \rangle/2$, and mean-square current density, $J = \langle \mathbf{j}^2 \rangle/2$, as B_0 increases (Fig. 1(b)). Since these quantities are a measure of the small-scale structure of the flow, this suggests that B_0 inhibits the development of such structures, at least in the direction parallel to $\mathbf{B}_0$. Furthermore, because the energy dissipation is proportional to $\Omega + J$, increasing B_0 also leads to decreased dissipation. At low B_0, $J(t) > \Omega(t)$, but as B_0 increases they become approximately equal; this is a consequence of the Alfvén effect holding mode by mode, since, e.g., $2J \equiv \sum k^2 |\mathbf{b}(\mathbf{k})|^2$.

We measure the anisotropy associated with a flow using the Shebalin angles, θ_Q [1, 2], defined by

$$\tan^2 \theta_Q = \frac{\Sigma\, k_\perp^2 |\mathbf{Q}(\mathbf{k}, t)|^2}{\Sigma\, k_z^2 |\mathbf{Q}(\mathbf{k}, t)|^2}, \tag{3}$$

where $k_\perp^2 = k_x^2 + k_y^2$, $\mathbf{Q}$ is any one of the fields $\mathbf{v}$, $\boldsymbol{\omega}$, $\mathbf{a}$, $\mathbf{b}$, $\mathbf{j}$, and the summations extend over all wavevectors. A physical interpretation of $\tan^2 \theta_Q$ is as the ratio

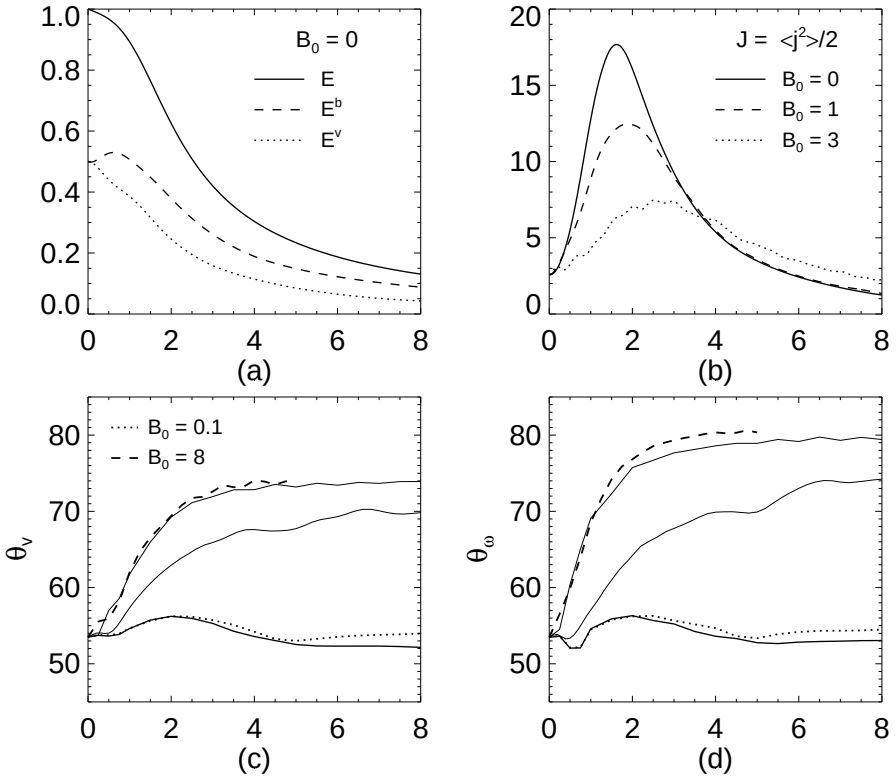

Fig. 1. Time histories for some quantities associated with the incompressible runs. The horizontal coordinate is always time. (a) Energies for the $B_0 = 0$ run; (b) mean-square current densities; (c)–(d) Shebalin angles as a function of B_0. Each curve is for a distinct value of B_0. In general stronger anisotropies correspond to larger B_0. Unique linestyles are used where ambiguity is possible. Angles are in degrees.

of a weighted mean-square perpendicular wavenumber to its parallel counterpart, the weighting factor being the 'energy' spectrum for $\mathbf{Q}$. It follows that an isotropic spectrum has $\theta_Q = \tan^{-1}\sqrt{2} \simeq 54.74°$, while a field with all excited modes perpendicular to $\mathbf{B}_0$ has $\theta_Q = 90°$.

In Fig. 1(c–d) plots of $\theta_v(t)$ and $\theta_\omega(t)$ are shown, each curve corresponding to a different value of B_0 (the equivalent plots for $\theta_b(t)$ and $\theta_j(t)$ are very similar [2]). Although the angles fluctuate, the overall trend is an increase with time, initially quite a rapid one. In the range $1/2 \lesssim B_0 \lesssim 3$, the anisotropy increases with B_0, with saturation occuring above this range. At low B_0 the field is too weak to significantly influence the flow's natural isotropy, while at high B_0 a rough saturation with time is also evident, but the level may well be affected by the strength of the turbulence since higher Reynolds numbers will lead to

longer periods of fully developed turbulence. It is also the case that at fixed time, $\theta_v < \theta_\omega$ and $\theta_a < \theta_b < \theta_j$. This is interpreted as indicating that the smaller scales are more anisotropic [1, 2, 5].

We stress that the development of the anisotropy is a *non*linear process. Runs for which the nonlinear terms are set to zero have Shebalin angles that show no significant evolution, i.e., they stay approximately isotropic. The situation considered by Moffatt [6], where $\nu \gg \eta$, is distinct from that considered here ($\nu = \eta$) for both the linearized and nonlinear dynamics. In particular, the dispersion relation obtained from the linearized equations in the equal Reynolds number case is isotropic. To emphasize the nonlinear nature of the process we show in Fig. 2 contour plots of the energy spectrum, $E(k_\perp, k_\parallel)$, at $t = 0$ and 1.5, for the $B_0 = 3$ run. Clearly spectral transfer is (relatively) accelerated in the perpendicular direction. Similar plots for the $B_0 = 0$ run show no such asymmetry.

It should also be noted that dissipation is crucial to the persistence of the anisotropies [1, 2]. Initially ideal runs evolve very similarly to their dissipative analogs; after a few turnover times, however, the anisotropy starts a slow decay back towards isotropy. This is a consequence of the statistical mechanics of the finite-dimensional ideal systems [7]. The features and trends mentioned in this section were also seen in the 2D DNS study [1].

3 Compressible Results

Direct simulations of the compressible MHD equations with a polytropic equation of state ($p \propto \rho^{5/3}, \rho$ the density) have also been performed, for a range of initial conditions. Here we consider four such runs, all having $B_0 = 1$, and $\nu = \eta = 1/250$. Run c27 is the baseline incompressible run, with initial $\mathbf{v}$ and $\mathbf{b}$ similar to those described above. Runs s01 and s02 are identical to c27 at $t = 0$, with the addition of a uniform density field which is evolved thereafter according to the equation of continuity. Thus, the velocity fluctuations are initially purely solenoidal in these runs. As they also have small sonic Mach numbers ($M_s \leq 0.5$) they are referred to as *nearly* incompressible (NI), in distinction from weakly compressible (WC) initial data which also has small M_s, but no restriction on the nature of the velocity fluctuations. Run s06 is a WC run with $\mathbf{v}(t = 0)$ being purely longitudinal ($\mathbf{v}(\mathbf{k}) \parallel \mathbf{k}$).

Figure 2 shows θ_v and θ_ω for the four runs. Clearly there is very little difference between the θ_ω curves, and this is also true for θ_a, θ_b, and θ_j plots. The Shebalin angles for ρ and $\mathbf{v}$, however, display significant differences between the runs. The figure indicates that as M_s decreases, θ_v for the NI runs approaches the incompressible results from below. The anisotropy still develops for the longitudinal initial conditions (s06), but at a reduced level relative to the NI runs. In fact, plots of the Shebalin angles for the longitudinal and solenoidal components of $\mathbf{v}$ show that the former remains approximately isotropic for all the compressible runs, while for all four runs the solenoidal components are anisotropic and approximately equal. Interestingly, θ_ρ is anisotropic for the NI

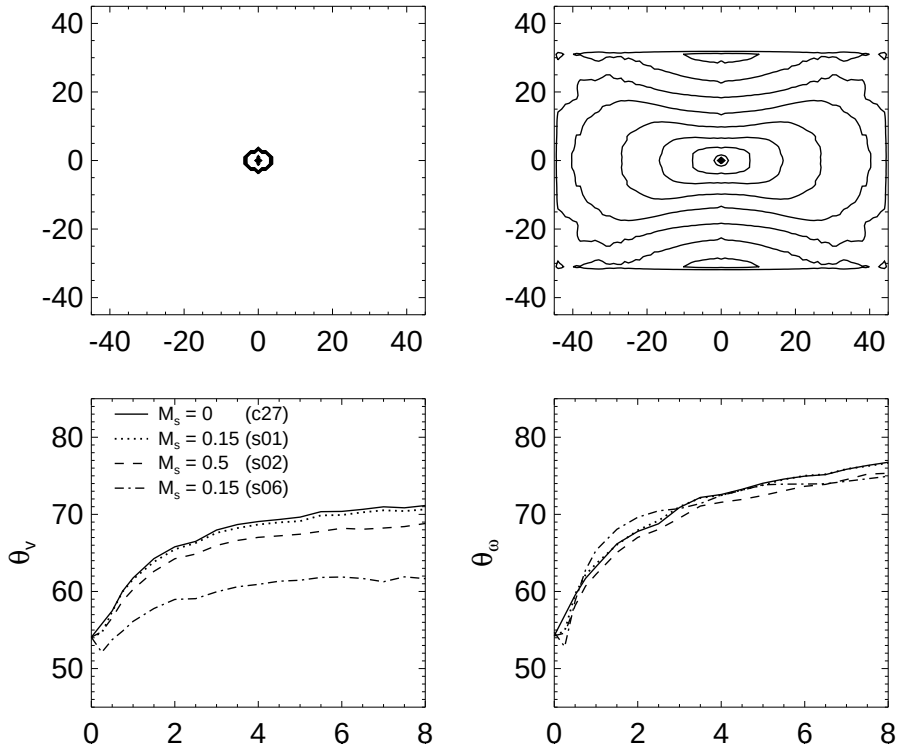

Fig. 2. Top panels: Contour plots of $\log E(k_\perp, k_\parallel)$ at $t = 0$ and 1.5 for the *in*compressible $B_0 = 3$ run. The horizontal coordinate is $k_\perp$, and 8 equally spaced contours are used. Lower panels: Some Shebalin angles for the weakly compressible runs as a function of time. All runs have $B_0 = 1$.
[NB: In the published verson of the paper, the top right figure was actually for $t = 2$, rather than $t = 1.5$. The figure is correct here. Jan 2003]

runs but isotropic for the longitudinal run. Taken together with the isotropic character of the longitudinal portion of the velocity fluctuations, this suggests that the density fluctuations are predominantly associated with pseudosound disturbances [8, 9] in the NI runs, while in the WC run they are dominated by genuine acoustic fluctuations.

4 Summary and Discussion

Our results indicate that a dc magnetic field imposed on 3D MHD turbulent flows induces anisotropic spectral transfer, with a relative enhancement for modes perpendicular to B_0. Measured in terms of ratios of $\perp$ and $\parallel$ correlation lengths, the anisotropies tend to increase with (a) B_0, (b) wavenumber, (c) Reynolds numbers, (d) time, and (e) decreasing $|H_c/E|$, with saturations occuring for large

enough B_0 and t. This behaviour is in complete qualitative agreement with the earlier 2D results [1]. Quantitatively, the value of B_0 above which saturation of the anisotropy occurs is slightly larger for the 3D case, presumably because of the extra (perpendicular) degree of freedom associated with this geometry.

A physically appealing explanation for the development of the (incompressible) anisotropy, based on a weak turbulence analysis of (1–2), was given in [1]. By computing the first-order nonlinear corrections to the solutions of the linearized equations, they showed that two excited Fourier modes ($\mathbf{k}_1$ & $\mathbf{k}_2$) will resonate effectively with a third, initially unexcited mode, only if (i) the excited modes are oppositely propagating, and (ii) either $\mathbf{k}_1$ or $\mathbf{k}_2$ is perpendicular to $\mathbf{B}_0$. Since also $\mathbf{k}_3 = \mathbf{k}_1 + \mathbf{k}_2$, modes with increased perpendicular components (relative to $\mathbf{k}_1$ and $\mathbf{k}_2$) can be excited, but not those with increased parallel components. Clearly, such excitations will transfer energy perpendicular to $\mathbf{B}_0$ in k-space, but not parallel to it. The argument readily generalizes to the 3D geometry. Recently, however, its relevance has been questioned in a formal perturbation theory approach [10, 11] that entirely ignores the 2D component of the fluctuations [12], and therefore excludes the essential physics of the above model for anisotropic spectral transfer [1].

A similar investigation of the 3D incompressible equations has been performed using a shell model based on the DIA equations [5]. Therein it is shown that the anisotropy of the inertial range energy saturates at Reynolds numbers $\sim 10^5$, and thus so does the total anisotropy since at large Reynolds numbers the inertial range contribution dominates. Their large Reynolds numbers saturation level is some 5° below the saturation level we find at fixed (and low) Reynolds number but large B_0 (our definition of the anisotropy angle differs from theirs but this has been taken into account). Because of the different initial conditions used and our much lower Reynolds numbers it is difficult to make direct comparisons between the two sets of results. Nonetheless, their initial data has a significant value of the cross helicity and in [2] it is reported that increasing $|H_c|/E$ reduces the anisotropy levels, so that in this sense there is no inconsistency between the DNS and shell model results.

In another 2D study [13] it was noted that a sufficiently strong $\mathbf{B}_0$ is associated with suppressed development of small-scale structures in that direction. Nonetheless, it does not follow that the turbulence will be completely suppressed for large enough $\mathbf{B}_0$. The initially 3D MHD turbulence could be reduced to weakly coupled planes of 2D MHD turbulence, oriented perpendicular to $\mathbf{B}_0$. Our results are consistent with such behaviour (e.g., isotropy in the $\perp$ plane, parallel correlation lengths $>$ than $\perp$ ones). Furthermore, analytic work on NI MHD [14] shows that in the limit of strong $\mathbf{B}_0$, the compressible 3D MHD equations reduce to incompressible 2D equations. Given the ramifications and simplifications associated with such a reduction, elucidation of the development and role of anisotropy in turbulent MHD flows remains a high research priority.

Finally, as regards the NI results, their convergence towards the incompressible ones is encouraging, pointing to the relevance of the incompressible dynamics when the velocity fluctuations are only weakly non-solenoidal. Thus, if the Mach number is low and magnetoacoustic waves are strongly damped (as is believed

to be the case in the outer solar corona and in the solar wind, for example [15]), the **v** and **b** fluctuations will quickly become NI. The leading order solutions for such systems are the incompressible ones [16], and as these are better understood than the fully compressible solutions, we anticipate that the application of these results to the evolution of solar wind fluctuations will prove fruitful.

Acknowledgments. We thank R. Grappin, H.K. Moffatt, and D. Montgomery for valuable comments and criticisms offered at the meeting. This work was supported in part by the UK PPARC (SO), the NASA SPTP grants at Bartol (WHM) and NASA-Goddard (SG), and by NSF grant ATM-9318728. Major computational support provided by the San Diego and NASA-Goddard Supercomputing Centers.

References

1. J. V. Shebalin, W. H. Matthaeus, and D. Montgomery. *J. Plasma Phys.*, **29**, 525 (1983)
2. S. Oughton, E. R. Priest, and W. H. Matthaeus. *J. Fluid Mech.*, **280**, 95 (1994)
3. R. H. Kraichnan. *Phys. Fluids*, **8**, 1385 (1965)
4. A. Pouquet, U. Frisch, and J. Léorat. *J. Fluid Mech.*, **77**, 321 (1976)
5. V. Carbone and P. Veltri. *Geophys. & Astrophys. Fluid Dynam.*, **52**, 153 (1990)
6. H. K. Moffatt. *J. Fluid Mech.*, **28**, 571 (1967)
7. T. Stribling and W. H. Matthaeus. *Phys. Fluids B*, **2**, 1979 (1990)
8. W. H. Matthaeus and M. R. Brown. *Phys. Fluids*, **31**, 3634 (1988)
9. S. Ghosh and W. H. Matthaeus. *Phys. Fluids A*, **4**, 148 (1992)
10. S. Sridhar and P. Goldreich. *Astrophys. J.*, **432**, 612 (1994)
11. P. Goldreich and S. Sridhar. *Astrophys. J.*, **438**, 763 (1995)
12. D. C. Montgomery and W. H. Matthaeus. *Astrophys. J.*, in press (1995)
13. U. Frisch, A. Pouquet, P.-L. Sulem, and M. Meneguzzi. *J. de Mécanique Théorique et Appliquée*, **216**, 191 (1983)
14. G. P. Zank and W. H. Matthaeus. *J. Plasma Phys.*, **48**, 85 (1992)
15. A. Barnes. in *Solar System Plasma Physics*, ed. by E. N. Parker, C. F. Kennel, and L. J. Lanzerotti. Vol. I, page 251. North-Holland (1979)
16. G. P. Zank and W. H. Matthaeus. *Phys. Fluids A*, **5**, 257 (1993)